

# First-principles insights into the atomic structure of carbon-nitrogen-oxygen complex color centers in silicon

Péter Udvarhelyi<sup>1,\*</sup>

<sup>1</sup>*International Center for Young Scientists, National Institute for Materials Science, 1-1 Namiki, Tsukuba, Ibaraki, 305-044, Japan*

(Dated: March 4, 2026)

Spin-active color centers are the basis of solid-state defect systems utilized in quantum technologies. Although silicon is an emerging host material for quantum defects, there is an urgent need to characterize color centers with non-zero electron spin ground state in this platform, beside the prominent T-center. In this work, we carry out first-principles calculations to identify the possible atomic structures originating the experimentally observed N-line series in silicon. We propose that the core structure of the N1 center consists of a neighboring carbon and nitrogen interstitial atoms. Furthermore, we predict that more complex defects involving self-interstitial and interstitial oxygen atoms are feasible candidates for the further lines in the series. As all of these color centers are isoelectronic structures to the T-center, they provide a family of alternative spin doublet qubits with emission near the low-energy telecommunication bands.

## I. INTRODUCTION

Silicon is an emerging material platform for defect-based quantum technologies [1]. As one of the most technologically mature materials, it offers advantages in growth, microfabrication, and CMOS-compatible device integration [2, 3]. Recent advances in isotope engineering [4] and ion implantation techniques [5, 6] have positioned silicon as a promising host for quantum defects, joining the more established platforms of diamond and silicon carbide.

The family of carbon-related defects is the focus of recent experimental and theoretical investigations. Several such emitter centers were identified to operate in the telecommunication wavelength ranges. The notable mentions are the interstitial carbon defect ( $C_i$ ) [7, 8], the G-center ( $C_sC_i$ ) [9, 10], the C-center ( $C_iO_i$ ) [10, 11], and the T-center ( $C_sC_iH_i$ ) [12, 13], where  $s$  and  $i$  subscripts label substitutional and interstitial defect positions, respectively. The latter is the prominent defect possessing a non-zero spin in its ground state [2, 14, 15]. Despite its promising spin and optical properties, the involvement of a single hydrogen passivation in the color center makes its deterministic creation challenging [13]. Recent theoretical studies proposed alternative structures to circumvent this problem by searching for isoelectronic defect structures to the T-center. In these approaches, the CH part of the CCH defect is replaced with a trivalent atom from the boron group (B, Al, Ga, and In) [16]. Building on previous calculation results on carbon-nitrogen defect complexes [17–19], it was recently proposed that nitrogen can work as a simple replacement as well [20]. The latter work predicted the  $C_sN_i$  defect in its split dumbbell configuration as a novel, T-center-like telecom emitter in silicon, despite its larger formation energy compared to its dissociated neighbor form.

In this work, we focus on identifying the atomic origin of the N-line series in silicon, labelled by the N1, N2, N3, N4, and N5 zero phonon lines (ZPL), which are positioned closely at 745.6, 758.0, 761.5, 767.4, and 772.4 meV, respectively [21, 22]. The lines were only observed after carbon and nitrogen co-implantation, suggesting the incorporation of these two elements in the centers. Comparing the FZ and CZ silicon samples, oxygen incorporation is only possible in the N3, N4, and N5 lines. Isotope shift measurements of the ZPL lines are consistent with the involvement of a single nitrogen and a single carbon atom in the core of the defect centers. Thermal annealing effect on the photoluminescence identified the N1 center as the most stable of the set, followed by N2, while the oxygen-related lines disappear first with increasing temperature. Experiments focusing on the N1 center revealed that ion implantation is crucial for the formation of the defect, as the line cannot be observed in nitrogen-doped and electron-irradiated samples [23]. They also reveal the bound exciton nature of the optical transition and Zeeman-splitting of the N1 line, consistent with a spin 1/2 defect state. Consequently, the color center is in its neutral charge state, and the spin originates from the odd number of electrons in the C-N complex. The N1 transition couples to two local vibrational modes (LVM) at 71.3 meV and 122.9 meV with respect of the N1 ZPL energy [24, 25]. Furthermore, an exceptionally strong optical coupling of the defect center to the  $O^\Gamma$  vibronic band is observed. Uniaxial stress measurements on the ZPL shift revealed the point symmetries of  $C_{1h}$  for N1 and N5, and  $C_1$  for N2 and N3, respectively [26]. The stress responses also show a slight change between the N1 and N2 core structures and a smaller perturbation from oxygen. It is concluded that the color centers consist of two slightly different C-N cores, N1 and N2, and their perturbations by additional oxygen incorporation create N5 and N3, respectively. There are no further experimental findings available for the N4 line of the series owing to its relatively weak photoluminescence inten-

\* udvarhelyi.peter@nims.go.jp

sity. Although there is strong experimental evidence on the composition and point symmetries of the N-centers, their exact atomic configuration and electronic structure remain unidentified.

In this work, we demonstrate that the atomic structures of C-N, C-N-Si, C-N-O, and C-N-Si-O defect stoichiometries showing the lowest formation energy and largest binding energy possess electronic and optical properties in reasonable agreement with the experimental findings on the N-lines. Moreover, these color centers are isoelectronic to the T-center, and as such, all possess a spin-doublet ground state.

## II. METHODS

We employ density functional theory (DFT) calculations with a plane-wave basis and periodic supercells as implemented in the Quantum Espresso code [27–29]. The core electrons are treated in the pseudopotential method using the Optimized Norm-Conserving Vanderbilt (SG15 ONCV) potentials [30, 31]. GGA density functionals of Perdew-Burke-Ernzerhof (PBE) [32] and the hybrid functional of Heyd-Scuseria-Ernzerhof (HSE06) [33] were used for configuration pre-screening and final results, respectively. The optimized lattice constant of the cubic Bravais-cell of the silicon host is 5.477 Å and 5.446 Å using PBE and HSE06 functional, respectively. The calculations are performed in a 216-atom,  $3 \times 3 \times 3$  silicon supercell using  $\Gamma$ -point sampling and 80 Ry plane-wave cutoff. Convergence tests for the zero phonon line (ZPL) transition energies were calculated in a 512-atom,  $4 \times 4 \times 4$  silicon supercell using the HSE06 functional with decreased plane-wave cutoff to 60 Ry to tackle the computational overhead in this large cell. Ionic relaxation with a force threshold of 0.001 a.u. was carried out in all DFT calculations. Excited states were calculated and relaxed using the  $\Delta$ SCF method of fixed occupations [34]. Total energies in charged supercells were corrected using the method of Freysoldt *et al.* [35]. Formation energies at charge state  $q$  were calculated as

$$E_{\text{form}}^q = E_{\text{defect}}^q - E_{\text{host}} - \sum_i \mu_i n_i + qE_{\text{Fermi}}, \quad (1)$$

where  $\mu_i$  is the chemical potential derived from silicon, diamond,  $\text{N}_2$ , and  $\text{O}_2$ , while  $n_i$  is the number of defects of species  $i$  created in the host material. Optical transition dipoles ( $\mu$ ) were calculated in the ground state configurations using time-dependent density functional theory (TDDFT) within the Tamm-Dancoff approximation and PBE functional [32] as implemented in the WEST code [36]. Optical lifetimes ( $\tau$ ) from the transition dipole moments are calculated using the Wigner-Weisskopf formula [37]

$$\frac{1}{\tau} = \frac{2(2\pi)^3 n_r E_{\text{ZPL}}^3 |\mu|^2}{3\epsilon_0 h^4 c^3}, \quad (2)$$

where  $n_r = 3.42$  is the refractive index of the silicon crystal,  $E_{\text{ZPL}}$  is the experimental ZPL energy of the associated optical transition,  $\epsilon_0$  is the vacuum permittivity,  $h$  is the Planck constant, and  $c$  is the speed of light. A volume-dependent scaling factor of  $V/\pi a_0^3$  was applied to the calculated  $|\mu|^2$ , where  $a_0 = 12.6$  Å is the Bohr radius of the heavy hole in the valence band [20]. Phonon properties of the defects were calculated in the 216-atom supercell using density functional perturbation theory (DFPT) at the PBE level in Quantum Espresso. Localized vibration modes were identified by calculating the inverse participation ratio (IPR) of atomic vibration normal modes  $\mathbf{u}_i$  using

$$\text{IPR} = \frac{1}{\sum_i (|u_i|^2)^2}. \quad (3)$$

The partial Huang-Rhys factors ( $S_i$ ) are calculated using the ionic position differences from the HSE ground ( $\mathbf{R}_{g,I}$ ) and excited states ( $\mathbf{R}_{e,I}$ ), projected on the phonon modes ( $\mathbf{e}_{i,I}$ )

$$Q_i = \sum_I \sqrt{m_I} \mathbf{e}_{i,I} \cdot (\mathbf{R}_{e,I} - \mathbf{R}_{g,I}), \quad (4)$$

$$S_i = \frac{\omega_i}{2\hbar} Q_i^2, \quad (5)$$

where  $\omega_i$  is the normal frequency of the corresponding normal mode  $i$ . The Debye-Waller factor (DWF) is calculated as

$$\text{DWF} = \exp\left(-\sum_i S_i\right). \quad (6)$$

The phonon sideband is simulated from  $S_i$  using the generator function approach of Alkauskas *et al.* [38]. Atomic structures are visualized using the VESTA code.

## III. RESULTS

To unveil the atomic structure of the N-lines in silicon, we systematically explore the interactions between the experimentally associated atomic species. First, we focus on formation and thermal stability. We search for defect configurations with the most favorable energetics as candidates for further investigations. By gradually increasing the complexity of the models, we explore interactions among C-N, C-N-Si, C-N-O, and C-N-Si-O. Finally, we compare the detailed calculations on the electronic and optical properties of the most stable defect configurations to previous experiments.

### A. Aggregation of neutral carbon and nitrogen atom pairs

Carbon-related impurities are the principal constituents of the recently studied color centers in sili-

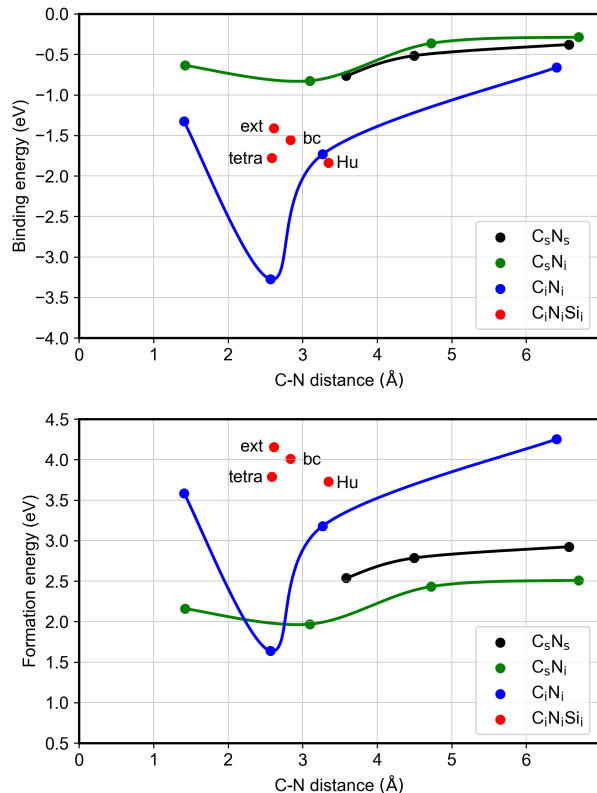


FIG. 1. Binding and formation energy plots of carbon and nitrogen interactions in silicon as a function of the interatomic distance. The lines connecting the calculation points in equilibrium geometries are interpolations to guide the eye along the pair formation path. For the three-center interstitial defects of C-N-Si (red), only the lowest energy configurations are shown for each defect motif (see Sec. III B). The corresponding structures of the latter are visualized in Fig. 2

con. Although their aggregation has been studied in detail [39], their interaction with nitrogen defects needs further investigation. Given that the base structure of the N-centers consists of a single carbon and a single nitrogen atom, we focus on interactions between such pairs occupying various sites in the silicon lattice. As the bound exciton transitions and the doublet spin observed in experiments suggest a neutral ground state, and both carbon and nitrogen have a large window of stability in their neutral charge states in silicon (see Fig. 7), we constrain our investigations to neutral-pair interactions in binding energy calculations, formulated as

$$E_{\text{binding}}^0 = (E_{\text{product}}^0 + E_{\text{host}}) - (E_{\text{defect1}}^0 + E_{\text{defect2}}^0), \quad (7)$$

where negative binding energy corresponds to a stable product complex. This assumption is further justified by the convergence observed for the cases where several equilibrium points along the dissociation path are calculated. The only exception is the C-N-Si interaction, where several candidates can be considered based only on their formation and stability (see Sec. III B for more

detail).

The results are collected in Fig. 1, where binding and formation energies are plotted as a function of the carbon-nitrogen distance in the defect complex. The calculation points correspond to equilibrium defect configurations, while the connecting interpolated curves are shown to guide the eye along the dissociation path towards the most favorable structures (minima points). Focusing only on the carbon-nitrogen structures first, we can see that the substitutional pair complex is unfavored in formation energy compared to the C<sub>s</sub>N<sub>i</sub> complex. This follows from the formation energy difference between the isolated N<sub>s</sub> and N<sub>i</sub> defects. The energetically most favorable configuration of the C<sub>s</sub>N<sub>s</sub> defect is the neighboring pair in C<sub>3v</sub> symmetry. The most compact structure of the C<sub>s</sub>N<sub>i</sub> complex is the split dumbbell configuration, which was recently predicted as a novel emitter defect [20]. However, this configuration is metastable, as its first dissociation step results in the energetically most favorable complex of a neighboring C<sub>s</sub> and split-dumbbell N<sub>i</sub> defect. This defect shows no symmetry (C<sub>1</sub>) consistent with breaking the C<sub>1h</sub> symmetry of the isolated split dumbbell N<sub>i</sub> by the adjacent C<sub>s</sub> defect. Its counterpart of a neighboring C<sub>i</sub>N<sub>s</sub> defect is proven to be unstable toward reconfiguration to the former complex in our calculations.

Finally, we find that the C<sub>i</sub>N<sub>i</sub> defect complex is the global minimum configuration in the carbon-nitrogen pair-interaction space. Although its dissociated forms show larger formation energies, this is consistent with the formation of the N-series only observed under ion carbon-nitrogen co-implantation conditions. Despite the hindered formation path, their aggregation is strongly driven by the huge binding energy of the complex. Analysing the structures along the dissociation path, we find the most compact metastable bond-centered pair, then at the global minimum, the neighboring split dumbbell configuration. This latter structure is analogous to the C-center (C<sub>i</sub>O<sub>i</sub>) [40]. The last notable structure is at the next dissociation step, resulting in the second neighbor split pair configuration, where the silicon dangling bonds of the pair reconstruct to form a Humble-structure. Based on its exceptional stability among the C-N defect configurations, we select the C<sub>i</sub>N<sub>i</sub> complex as the candidate for the N1 core structure, which shows the largest thermal stability among the N-lines in experiments. Next, we search for defect candidates for the N2 core structure.

## B. Motif-based search for the reaction involving self-interstitials

As experimental findings suggest that no additional impurity species are involved in the formation of the N2 center, we constrain our search to the involvement of an additional self-interstitial atom. Because of the close energy range of the stable isolated Si<sub>i</sub> defect configurations (see Fig. 7), the reaction path for the C<sub>i</sub>N<sub>i</sub>Si<sub>i</sub> complex is more complicated than the one-dimensional dissocia-

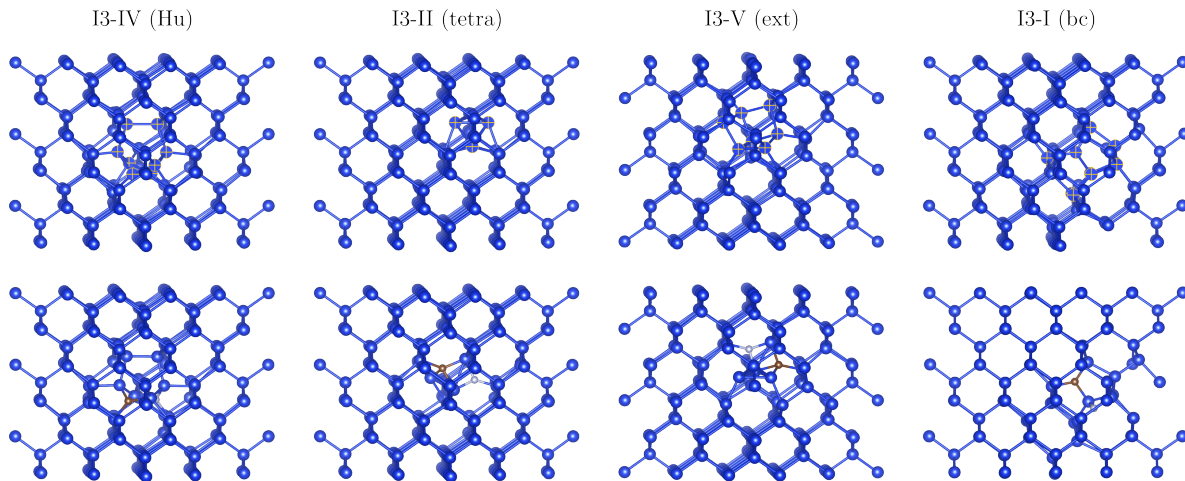


FIG. 2. Structural motifs of the lowest energy tri-interstitial silicon aggregates (upper row) serving as templates for the  $C_iN_iSi_i$  complex defect search. The resulting lowest energy configurations are shown under each parent motif. Si, N, and C atoms are drawn in dark blue, light blue, and brown, respectively.

tion path projections examined before. The large variety of the self-interstitial positions is also reflected in their aggregation. Previous calculations on tri-interstitial aggregations identified four low-energy structures [41–43]. These are the I3-I bond-centered (bc), I3-II tetrahedral (tetra), I3-IV Humble (Hu), and I3-V extended (ext) shown in the upper row of Fig. 2. Given the complexity of the possible interaction space, we assume that a motif-based search starting from the four lowest energy self-interstitial aggregate structures, and replacing two silicon atoms in their core structure with a carbon and a nitrogen atom, will result in the lowest energy structures of the  $C_iN_iSi_i$  complex. This method indeed results in four compact structures close in energy (see Fig 1). The corresponding structures with the largest binding energies are visualized under their parent I3 defect motifs in Fig. 2. We define the binding energy of the additional self-interstitial defect with respect to the isolated  $C_iN_i$  core structure and the isolated self-interstitial in their neutral charge states. As the "extended" and "tetra" labelled structures result in a large modification of the electronic structure of the  $C_iN_i$  core (see explanation in section III D), we select the bond-centered "bc" and Humble "Hu" structures as promising candidates for the  $C_iN_iSi_i$  defect core when interactions with interstitial oxygen is concerned in the next section.

### C. Oxygen interaction with the carbon-nitrogen complex defects

Strain experiments on the N-lines suggest that the role of oxygen in the N3, N4, and N5 centers is rather a perturbation effect on the corresponding oxygen-free N1 and N2 core structures. Furthermore, oxygen occupies a bond-centered interstitial position in the lattice, making

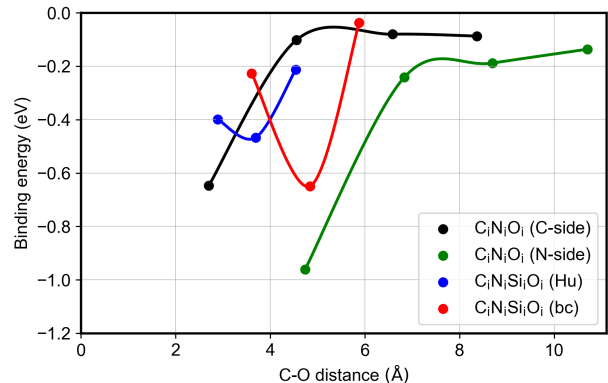


FIG. 3. Binding energy plot of oxygen interactions with the core structures of selected N1 and N2 candidate defects in silicon as a function of the C-O distance. The lines connecting the calculation points in equilibrium geometries are interpolations to guide the eye along the pair-formation path.

its aggregation path straightforward to follow. We model this by placing  $O_i$  at all the bond center positions around the core structures of the selected N1 and N2 candidates up to the second neighbor shell. From the calculation results, we identify the lowest energy configurations and the immediate aggregation paths around them. These selected paths are visualized in Fig 3, where the binding energy of the additional oxygen is plotted as a function of the C-O distance. We select four structures with large oxygen binding energy, and label them as the  $C_iN_iO_i$  (N-side),  $C_iN_iO_i$  (C-side),  $C_iN_iSi_iO_i$  (bc), and  $C_iN_iSi_iO_i$  (Hu), where "C-side" and "N-side" labels refer to the preferred aggregation direction of  $O_i$ , while "bc" and "Hu" refer to the N2 core structure configurations.

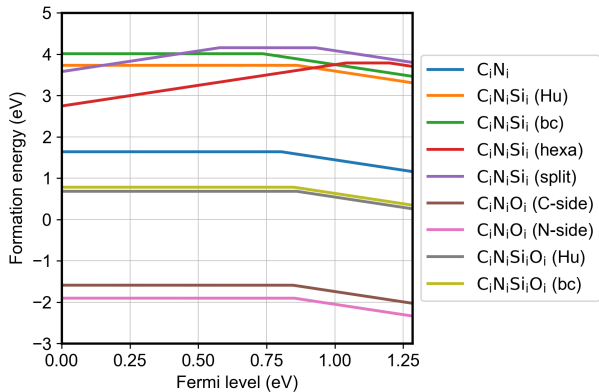


FIG. 4. Calculated formation energy diagram in the silicon bandgap for the candidate defects with the largest binding energies. The search for candidates with a single stable transition level compatible with pseudo-acceptor bound exciton centers rules out  $C_iN_iSi_i$  (hexa) and (split) configurations.

#### D. Electronic and optical properties

After we collected the most stable defect candidates, as evidenced by their large binding energies, we continued to filter them based on their electronic-structure compatibility with the N-lines. The calculated formation energy diagram in Fig. 4 shows several structures with only a single stable acceptor level. These are in good match with the bound-exciton origin of the N centers. We can rule out candidates with both donor and acceptor levels active [ $C_iN_iSi_i$  (hexa) and (split)], as this would lead to competing exciton transition processes in the color centers. We can consider the  $C_iN_i$  defect, the energetically most favorable, simplest core structure of the N-series, as the origin of the N1 line. From the remaining two contenders for the N2 center, we select  $C_iN_iSi_i$  (Hu) as its charge transition level position is at higher energies compared to the  $C_iN_i$  defect, in-line with the higher transition energy of the N2 line. The oxygen-containing candidates considered here all possess electronic structures compatible with the bound exciton transition.

Next, we focus on the optical properties of the  $C_iN_i$  defect. Its calculated ZPL energy of 701 meV slightly underestimates the experimental N1 ZPL at 745.6 meV. The calculation in a larger, 512-atom ( $4 \times 4 \times 4$ ) supercell resulted in a 779 meV ZPL energy. Linear extrapolation on these two datapoints can estimate the dilute ZPL energy limit of 836 meV. A similar systematic shift of the transition energies was reported in T-center-like electronic structures using the HSE06 functional [20], and the experimental ZPL energy can be expected to lie between the values calculated in the 512 and 216 atom models. Our calculations align with this trend. Furthermore, the calculation method using the PBE0 functional with a mixing parameter of 0.136 is proposed to be better suited for the T-center-like defects [20]. This method results in a 599 meV ZPL energy for the  $C_iN_i$  defect in the

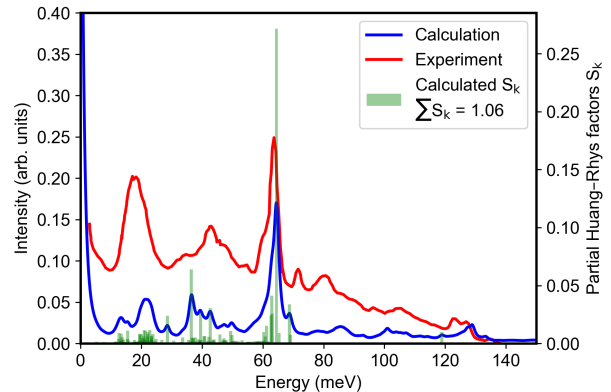


FIG. 5. Comparison of the calculated phonon sideband (blue) of the  $C_iN_i$  defect to the experimental sideband of the N1 emitter reported in Ref. 24 (red). Two localized vibration modes are identified in the calculated spectrum at 66.8 meV and 118.9 meV. The calculated total Huang-Rhys factor of 1.06 corresponds to a Debye-Waller factor of 0.35.

216-atom model. Applying this energy shift to the dilute limit approximated above gives 734 meV for the ZPL energy, which is in line with the HSE06 trends explained above, and is in close agreement with the experimental N1 ZPL energy.

To identify the N1 center, we use further experimental fingerprints from its optical sideband spectrum. The comparison of the calculated and measured sidebands of the  $C_iN_i$  defect and the N1 center plotted in Fig. 5 shows good agreement. We highlight the exceptionally strong coupling to the  $O^F$  band, and the identified LVM energies at 66.8 meV and 118.9 meV in close match with experiments. Based on these findings, we identify the most stable  $C_iN_i$  structure of the carbon-nitrogen pair in silicon as the origin of the N1 ZPL line. Moreover, we calculate a relatively large Debye-Waller factor (DWF) of 0.35 for this defect and an optical lifetime of 168 ns. These calculated values compare favorably to the experimental 0.23 DWF and 940 ns optical lifetime reported for the T-center [2]. These optical properties make the N1 center a strong contender for quantum photonics among bound-exciton telecom emitters in silicon.

The calculated ZPL transition energies for the other candidates lie close to that of the  $C_iN_i$  defect. The calculated relative energy shifts ( $\Delta ZPL$ ) with respect to the  $C_iN_i$  ZPL are 20, 23, and 25 meV for the  $C_iN_iSi_i$  (Hu),  $C_iN_iO_i$  (C-side), and (N-side), respectively. This shows possible matches with the N2, N4, and N5 line energy order. The assignment of the lines is further strengthened by the matching point symmetries for the N2 and N5 lines. For the origin of the missing N3 line, a straightforward choice could be the  $C_iN_iSi_iO_i$  (Hu) and  $C_iN_iSi_iO_i$  (bc) structures, both showing matching symmetry with N3. However, their calculated ZPL energies lie further apart from the formerly assigned ones ( $\Delta ZPL$  of 0 and 3 meV, respectively). This discrepancy makes it difficult

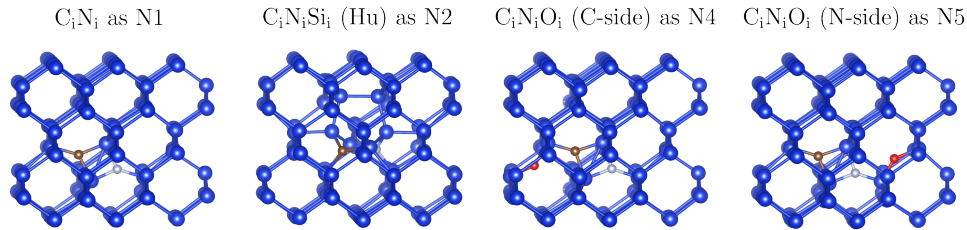


FIG. 6. Geometric structures of the calculated interstitial aggregate complexes with the strongest binding energies in their respective atomic constitution. Based on their point symmetry and calculated optical properties, they are assigned as the origin of several color centers in the experimental N-line series. Dark blue, light blue, brown, and red balls represent Si, N, C, and O atoms, respectively.

to make predictions on the origin of the N3 line.

Our calculations on the optical properties of the candidate structures conclude with strong evidence for the  $C_iN_i$  defect as the origin of the N1 center. Moreover, all the candidate structures lie in a 25 meV range of the former ZPL energy, suggesting that they are possible origins of the further lines in the N-series. Considering point symmetries and relative stabilities, we propose the assignment of the N2, N4, and N5 lines, while further studies on the formation path and optical properties of oxygen-related centers are suggested to identify the missing N3 ZPL line. The final candidate structures assigned to the N-centers are collected in Fig. 6.

#### IV. CONCLUSION

We applied first-principles calculations on complex defects consisting of carbon, nitrogen, oxygen, and self-interstitial defects in silicon. We find that the neighboring nitrogen-carbon interstitial pair ( $C_iN_i$ ) shows the smallest formation energy and the largest binding energy among the various structures of carbon-nitrogen pairs in silicon. Its exceptional stability,  $C_{1h}$  symmetry, electronic structure, ZPL energy, phonon sideband features, and LVM energies all show good agreement with the experimental properties of the N1 color center. Furthermore, our motif-based search for the involvement of an aggregated self-interstitial atom in the N1 core structure provides the optically active  $C_iN_iSi_i$  (Hu) defect with compatible symmetry and a reasonable ZPL energy shift to be assigned as the N2 center. By mapping the binding energies of an oxygen interstitial defect to the N1 core, similar considerations lead to the assignment of the most stable  $C_iN_iO_i$  (N-side) structure as the N5 center. Its metastable (C-side) variant is tentatively assigned to the N4 center by considering its matching smaller ZPL energy compared to N5 and its weak PL intensity in experiments, explained by its larger formation energy. Calculations on the origin of the N3 line could not be concluded. However, we propose the oxygen-modified  $C_iN_iSi_iO_i$  (Hu) and  $C_iN_iSi_iO_i$  (bc) structures as key candidates for further investigations. Our findings highlight

the family of N color centers in silicon as telecom emitters with desirable optical properties. Furthermore, all of the N-centers are isoelectronic to the T-center with a similar electronic structure, making them a promising alternative quantum bit. Our calculations provide valuable insight into the atomic structure origin of these color centers, paving the way for their further theoretical and experimental investigation.

#### ACKNOWLEDGEMENT

P.U. acknowledges the support from the ICYS fellowship and research fund at NIMS. This work was achieved through the use of the Supercomputer System SQUID at the D3 Center at Osaka University.

#### APPENDIX

The calculated charge transition levels for isolated single defects, which appear as constituents in larger complexes studied in this work, are plotted in Fig. 7. As carbon and nitrogen defects show a large stability re-

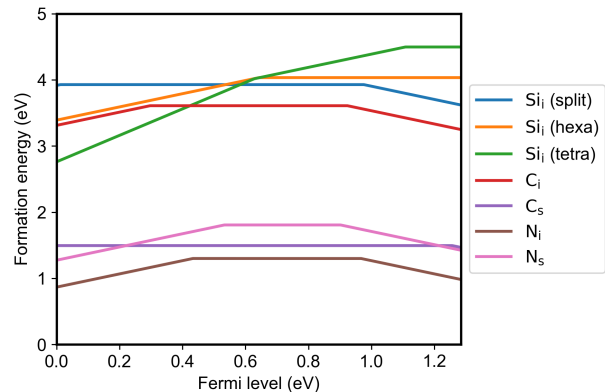


FIG. 7. Calculated formation energy diagram of single defect configurations in the silicon bandgap.

gion in their neutral charge state, we describe their aggregation energetics accordingly. While nitrogen is favorably formed as an interstitial defect, carbon atoms prefer to occupy lattice sites. However, the interstitial form of carbon impurities can be activated in a

self-interstitial-rich environment around large damage regions in the lattice. The driving force of this so-called Watkins replacement mechanism is the exothermic reaction of  $C_s + Si_i \rightarrow C_i$  [44–46]. These considerations provide the basis for the formation of C-N interstitial pairs in silicon.

- 
- [1] D. D. Awschalom, R. Hanson, J. Wrachtrup, and B. B. Zhou, Quantum technologies with optically interfaced solid-state spins, *Nature Photonics* **12**, 516 (2018).
- [2] L. Bergeron, C. Chartrand, A. T. K. Kurkjian, K. J. Morse, H. Riemann, N. V. Abrosimov, P. Becker, H.-J. Pohl, M. L. W. Thewalt, and S. Simmons, Silicon-integrated telecommunications photon-spin interface, *PRX Quantum* **1**, 020301 (2020).
- [3] J. Wang, F. Sciarrino, A. Laing, and M. G. Thompson, Integrated photonic quantum technologies, *Nature Photonics* **14**, 273 (2020).
- [4] D. Holmes, B. C. Johnson, C. Chua, B. Voisin, S. Kocsis, S. Rubanov, S. G. Robson, J. C. McCallum, D. R. McCamey, S. Rogge, and D. N. Jamieson, Isotopic enrichment of silicon by high fluence  $^{28}\text{Si}^-$  ion implantation, *Phys. Rev. Mater.* **5**, 014601 (2021).
- [5] G. Andrini, G. Zanelli, S. Ditalia Tchernij, E. Corte, E. Nieto Hernández, A. Verna, M. Cocuzza, E. Bernardi, S. Virzì, P. Traina, I. P. Degiovanni, M. Genovese, P. Olivero, and J. Forneris, Activation of telecom emitters in silicon upon ion implantation and ns pulsed laser annealing, *Communications Materials* **5**, 47 (2024).
- [6] M. Hollenbach, N. Klingner, P. Mazarov, W. Pilz, A. Nadzeyka, F. Mayer, N. V. Abrosimov, L. Bischoff, G. Hlawacek, M. Helm, and G. V. Astakhov, Programmable activation of quantum emitters in high-purity silicon with focused carbon ion beams, *Advanced Quantum Technologies* **8**, 2400184 (2025), <https://advanced.onlinelibrary.wiley.com/doi/pdf/10.1002/qrt.1024>.
- [7] K. Thonke, A. Teschner, and R. Sauer, New photoluminescence defect spectra in silicon irradiated at 100 k: Observation of interstitial carbon?, *Solid State Communications* **61**, 241 (1987).
- [8] P. Deák, S. Li, and A. Gali, Quantum bit with telecom wave-length emission from a simple defect in si, *Communications Physics* **7**, 337 (2024).
- [9] L. W. Song, X. D. Zhan, B. W. Benson, and G. D. Watkins, Bistable interstitial-carbon-substitutional-carbon pair in silicon, *Phys. Rev. B* **42**, 5765 (1990).
- [10] P. Udvarhelyi, B. Somogyi, G. Thiering, and A. Gali, Identification of a telecom wavelength single photon emitter in silicon, *Phys. Rev. Lett.* **127**, 196402 (2021).
- [11] G. Davies, Carbon-related processes in crystalline silicon, in *Defects in Semiconductors 15*, Materials Science Forum, Vol. 38 (Trans Tech Publications Ltd, 1989) pp. 151–158.
- [12] A. N. Safonov, E. C. Lightowers, G. Davies, P. Leary, R. Jones, and S. Öberg, Interstitial-carbon hydrogen interaction in silicon, *Phys. Rev. Lett.* **77**, 4812 (1996).
- [13] D. Dhaliyah, Y. Xiong, A. Sipahigil, S. M. Griffin, and G. Hautier, First-principles study of the t center in silicon, *Phys. Rev. Mater.* **6**, L053201 (2022).
- [14] D. B. Higginbottom, A. T. K. Kurkjian, C. Chartrand, M. Kazemi, N. A. Brunelle, E. R. MacQuarrie, J. R. Klein, N. R. Lee-Hone, J. Stacho, M. Ruether, C. Bowness, L. Bergeron, A. DeAbreu, S. R. Harrigan, J. Kanganayagam, D. W. Marsden, T. S. Richards, L. A. Stott, S. Roorda, K. J. Morse, M. L. W. Thewalt, and S. Simmons, Optical observation of single spins in silicon, *Nature* **607**, 266 (2022).
- [15] F. Islam, C.-M. Lee, S. Harper, M. H. Rahaman, Y. Zhao, N. K. Vij, and E. Waks, Cavity-enhanced emission from a silicon t center, *Nano Letters* **24**, 319 (2024), pMID: 38147350, <https://doi.org/10.1021/acs.nanolett.3c04056>.
- [16] Y. Xiong, J. Zheng, S. McBride, X. Zhang, S. M. Griffin, and G. Hautier, Computationally driven discovery of t center-like quantum defects in silicon, *Journal of the American Chemical Society* **146**, 30046 (2024), pMID: 39466834, <https://doi.org/10.1021/jacs.4c06613>.
- [17] A. Platonenko, F. S. Gentile, J. Maul, F. Pascale, E. A. Kotomin, and R. Dovesi, Nitrogen interstitial defects in silicon. a quantum mechanical investigation of the structural, electronic and vibrational properties, *Materials Today Communications* **21**, 100616 (2019).
- [18] N. Kuganathan, S.-R. G. Christopoulos, K. Papadopoulou, E. N. Sgourou, A. Chroneos, and C. A. Londos, A density functional theory study of the cin and the cinoi complexes in silicon, *Modern Physics Letters B* **37**, 2350154 (2023), <https://doi.org/10.1142/S0217984923501543>.
- [19] N. Kuganathan, E. N. Sgourou, N. Sarlis, A. Chroneos, and C. A. Londos, Nitrogen-related defects in crystalline silicon, *Applied Sciences* **14**, 10.3390/app14041631 (2024).
- [20] J. K. Nangoi, M. E. Turiansky, and C. G. Van de Walle, Carbon-nitrogen complex as an alternative to the t center in si, *Phys. Rev. B* **113**, L060101 (2026).
- [21] A. Dörnen, G. Pensl, and R. Sauer, Set of five related photoluminescence defects in silicon formed through nitrogen-carbon interactions, *Phys. Rev. B* **35**, 9318 (1987).
- [22] A. Dörnen, R. Sauer, and G. Pensl, Complexing of nitrogen with carbon and oxygen in silicon: Photoluminescence studies, *Journal of Electronic Materials* **17**, 121 (1988).
- [23] A. Dörnen, G. Pensl, and R. Sauer, Nitrogen-carbon radiative defect at 0.746 eV in silicon, *Phys. Rev. B* **33**, 1495 (1986).
- [24] A. Dörnen, R. Sauer, and G. Pensl, Nitrogen-carbon interactions in optical defects in silicon, *MRS Online Proceedings Library* **59**, 545 (1985).
- [25] A. Dörnen, G. Pensl, and R. Sauer, Vibrational mode nitrogen and carbon isotope shifts on the n1(0.746 eV) photoluminescence spectrum in silicon, *Solid State Communications* **57**, 861 (1986).

- [26] A. Dörnen, R. Sauer, and G. Pensl, Nitrogen-carbon-oxygen radiative centers in silicon: Uniaxial stress measurements, in *Defects in Semiconductors 15*, Materials Science Forum, Vol. 38 (Trans Tech Publications Ltd, 1989) pp. 631–636.
- [27] P. Giannozzi, S. Baroni, N. Bonini, M. Calandra, R. Car, C. Cavazzoni, D. Ceresoli, G. L. Chiarotti, M. Cococcioni, I. Dabo, A. D. Corso, S. de Gironcoli, S. Fabris, G. Fratesi, R. Gebauer, U. Gerstmann, C. Gougoussis, A. Kokalj, M. Lazzeri, L. Martin-Samos, N. Marzari, F. Mauri, R. Mazzarello, S. Paolini, A. Pasquarello, L. Paulatto, C. Sbraccia, S. Scandolo, G. Sclauzero, A. P. Seitsonen, A. Smogunov, P. Umari, and R. M. Wentzcovitch, Quantum espresso: a modular and open-source software project for quantum simulations of materials, *Journal of Physics: Condensed Matter* **21**, 395502 (2009).
- [28] P. Giannozzi, O. Andreussi, T. Brumme, O. Bunau, M. B. Nardelli, M. Calandra, R. Car, C. Cavazzoni, D. Ceresoli, M. Cococcioni, N. Colonna, I. Carnimeo, A. D. Corso, S. de Gironcoli, P. Delugas, R. A. DiStasio, A. Ferretti, A. Floris, G. Fratesi, G. Fugallo, R. Gebauer, U. Gerstmann, F. Giustino, T. Gorni, J. Jia, M. Kawamura, H.-Y. Ko, A. Kokalj, E. Küçükbenli, M. Lazzeri, M. Marsili, N. Marzari, F. Mauri, N. L. Nguyen, H.-V. Nguyen, A. O. de-la Roza, L. Paulatto, S. Poncé, D. Rocca, R. Sabatini, B. Santra, M. Schlipf, A. P. Seitsonen, A. Smogunov, I. Timrov, T. Thonhauser, P. Umari, N. Vast, X. Wu, and S. Baroni, Advanced capabilities for materials modelling with quantum espresso, *Journal of Physics: Condensed Matter* **29**, 465901 (2017).
- [29] P. Giannozzi, O. Baseggio, P. Bonfà, D. Brunato, R. Car, I. Carnimeo, C. Cavazzoni, S. de Gironcoli, P. Delugas, F. Ferrari Ruffino, A. Ferretti, N. Marzari, I. Timrov, A. Urru, and S. Baroni, Quantum ESPRESSO toward the exascale, *The Journal of Chemical Physics* **152**, 154105 (2020), [https://pubs.aip.org/aip/jcp/article-pdf/doi/10.1063/5.0005082/16721881/154105\\_1\\_online.pdf](https://pubs.aip.org/aip/jcp/article-pdf/doi/10.1063/5.0005082/16721881/154105_1_online.pdf).
- [30] D. R. Hamann, Optimized norm-conserving vanderbilt pseudopotentials, *Phys. Rev. B* **88**, 085117 (2013).
- [31] M. Schlipf and F. Gygi, Optimization algorithm for the generation of oncv pseudopotentials, *Computer Physics Communications* **196**, 36 (2015).
- [32] J. P. Perdew, K. Burke, and M. Ernzerhof, Generalized gradient approximation made simple, *Phys. Rev. Lett.* **77**, 3865 (1996).
- [33] A. V. Krukau, O. A. Vydrov, A. F. Izmaylov, and G. E. Scuseria, Influence of the exchange screening parameter on the performance of screened hybrid functionals, *J. Chem. Phys.* **125**, 224106 (2006).
- [34] A. Gali, E. Janzén, P. Deák, G. Kresse, and E. Kaxiras, Theory of spin-conserving excitation of the  $n-V^-$  center in diamond, *Phys. Rev. Lett.* **103**, 186404 (2009).
- [35] C. Freysoldt, J. Neugebauer, and C. G. Van de Walle, Fully ab initio finite-size corrections for charged-defect supercell calculations, *Phys. Rev. Lett.* **102**, 016402 (2009).
- [36] Y. Jin, V. W.-z. Yu, M. Govoni, A. C. Xu, and G. Galli, Excited state properties of point defects in semiconductors and insulators investigated with time-dependent density functional theory, *Journal of Chemical Theory and Computation* **19**, 8689 (2023), pMID: 38039161, <https://doi.org/10.1021/acs.jctc.3c00986>.
- [37] V. Weisskopf and E. P. Wigner, Berechnung der natürlichen linienbreite auf grund der diracschen lichttheorie, in *Part I: Particles and Fields. Part II: Foundations of Quantum Mechanics* (Springer Berlin Heidelberg, Berlin, Heidelberg, 1997) pp. 30–49.
- [38] A. Alkauskas, B. B. Buckley, D. D. Awschalom, and C. G. V. de Walle, First-principles theory of the luminescence lineshape for the triplet transition in diamond nv centres, *New Journal of Physics* **16**, 073026 (2014).
- [39] P. Deák, P. Udvarhelyi, G. Thiering, and A. Gali, The kinetics of carbon pair formation in silicon prohibits reaching thermal equilibrium, *Nature Communications* **14**, 361 (2023).
- [40] P. Udvarhelyi, A. Pershin, P. Deák, and A. Gali, An l-band emitter with quantum memory in silicon, *npj Computational Materials* **8**, 262 (2022).
- [41] A. Carvalho, R. Jones, J. Coutinho, and P. R. Briddon, Density-functional study of small interstitial clusters in si: Comparison with experiments, *Phys. Rev. B* **72**, 155208 (2005).
- [42] I. Santos, M. Aboy, P. López, L. A. Marqués, and L. Pelaz, Insights on the atomistic origin of x and w photoluminescence lines in c-si from ab initio simulations, *Journal of Physics D: Applied Physics* **49**, 075109 (2016).
- [43] Y. Baron, A. Durand, P. Udvarhelyi, T. Herzig, M. Khoury, S. Pezzagna, J. Meijer, I. Robert-Philip, M. Abbarchi, J.-M. Hartmann, V. Mazzocchi, J.-M. Gérard, A. Gali, V. Jacques, G. Cassabois, and A. Dréau, Detection of single w-centers in silicon, *ACS Photonics* **9**, 2337 (2022), <https://doi.org/10.1021/acsphotonics.2c00336>.
- [44] A. Bean and R. Newman, Low temperature electron irradiation of silicon containing carbon, *Solid State Communications* **8**, 175 (1970).
- [45] G. D. Watkins and K. L. Brower, Epr observation of the isolated interstitial carbon atom in silicon, *Phys. Rev. Lett.* **36**, 1329 (1976).
- [46] G. Davies, E. C. Lightowers, R. C. Newman, and A. S. Oates, A model for radiation damage effects in carbon-doped crystalline silicon, *Semiconductor Science and Technology* **2**, 524 (1987).